Structure and Activation Dynamics of RBL-2H3 Cells Observed with Scanning Force Microscopy

David Braunstein* and Annamma Spudich‡
*Department of Biochemistry and ‡Cell Sciences Imaging Facility and Department of Molecular and Cellular Physiology, Stanford University, Stanford, California 94305 USA

ABSTRACT Surface and subsurface dynamics of Rat Basophilic Leukemia cells, a model system of stimulated secretion, were imaged using Scanning Force Microscopy (SFM) at a rate of 50–60 s/image. Cytoskeletal elements and organelles were tracked within quiescent cells and those activated after IgE receptor crosslinking. In addition, surface waves were observed moving within the plasma membrane. The structures seen in quiescent and activated cells can be correlated with those seen in electron micrographs and topographic SFM images of fixed detergent-extracted cells. Furthermore, images of the detergent-extracted nuclei reveal the presence of numerous nuclear pore complexes. High-magnification images of the nuclear pore complexes show evidence of subunit structure and exhibit dimensions consistent with those reported previously using electron microscopy. The behavior and overall change in morphology of cells observed during activation was consistent with that observed under similar conditions with Differential Interference Contrast microscopy. This study demonstrates that SFM, unlike other techniques, can be used to provide high-resolution information in both fixed and living cells.

INTRODUCTION

The behavior of the cell surface is coupled to and reflects events within the cell interior (Stossel, 1993). Although traditional microscopies rely on the absorption or emission of radiation to generate image contrast, Scanning Force Microscopy (SFM), also known as Atomic Force Microscopy (AFM), senses differences in surface topography and compliance by tracking the deflection of a small sharp-tipped cantilever as it is scanned across the sample surface (Binnig et al., 1986). SFM's ability to image at high resolution in an ambient environment, ranging from atmospheric pressure to aqueous solution, has made it a very appealing tool for studying biological samples. The use of SFM has expanded beyond its initial use for imaging crystalline materials at near atomic resolution into the realm of soft biological samples, from small macromolecular assemblies (Weisenhorn et al., 1990; Hoh et al., 1993; Rees et al., 1993; Murray et al., 1993; Braunstein et al., 1993; Lyubchenko et al.; 1993; Allen et al., 1993) to whole cells (Henderson et al., 1992; Hörber et al., 1992). SFM permits one to study directly the changes undergone by the cell surface in response to changing conditions of the external medium. This capability promises to make SFM a powerful tool in studying the dynamics of the cell surface and its relationship to the underlying cytoskeleton.

We have used SFM to image the dynamics of organelles, cytoskeletal structures, and the cell membrane of live Rat Basophilic Leukemia (RBL-2H3) cells, a well characterized cell line that has been studied as a model system of stimulated secretion (Siraganian et al., 1982; Metzger et al., 1986). SFM can image cellular dynamics at higher resolution and definition than video microscopy, although with a relatively slow image acquisition rate (~50–60 s/image). Crosslinking the IgE receptors on the cell surface with a multivalent antigen, dinitrophenol-bovine serum albumin (DNP-BSA), initiates a chain of events that causes the secretion of histamine and serotonin (Metzger et al., 1986; Oliver et al., 1988) concomitant with rapid changes in the cytoskeleton and spreading of the cell across the sample substratum. Most (90%) of the RBL cells in a culture display changes in cell shape and cell motility when stimulated. These properties make this cell line an ideal candidate for using SFM to study the changes in the cell surface and the cytoskeleton initiated by signal transduction.

Before activation, RBL cells have a roughly spherical cell body, from which one or more long processes often extend. Upon activation, the periphery of the cells spreads and flattens within 3–5 min. This timescale of the activation-induced cellular response falls within the ~1 min/image acquisition rate of SFM. This feature, along with the higher resolution possible with SFM compared to video enhanced optical microscopy, allows the observation of many aspects of activation not possible with other techniques. The velocity of the structures seen in the live cell images are similar in magnitude to those measured for organelles in other systems. SFM topographic images of fixed detergent-extracted cytoskeletal preparations yield information consistent with electron micrographs (EMs) of similar preparations without the need for negative staining. With SFM, we correlated the structures imaged in live cells with those observed in topographic images of fixed detergent-extracted cytoskeletal preparations. Furthermore, we have observed key components of the nuclear membrane, nuclear pore complexes (NPCs) in situ, without negative staining. This study shows that SFM can be used to observe many aspects of the structure and dynamics

Received for publication 18 October 1993 and in final form 24 February 1994.

Address reprint requests to David Braunstein, Department of Biochemistry, Beckman Center, Stanford University Medical Center, Stanford, CA 94305-5307. Tel.: 415-725-6376; Fax: 415-725-2929; E-mail: braunste@cmgm.stanford.edu.

0006-3495/94/05/1717/09 $2.00

of cells normally studied with separate instruments, but with less perturbation than TEM and with greater resolution than video microscopy.

MATERIALS AND METHODS

Cell culture

RBL-2H3 cells were maintained as monolayer cultures as described previously (Spudich et al., 1992). Cells were harvested by trypsin treatment, diluted to 5×10^5 cells/ml, and sensitized with 0.5 μg/ml anti-DNP IgE (Sigma Chemical Co., St. Louis, MO). Aliquots of the sensitized cells were grown overnight on glass or Thermonox (Miles Scientific) coverslips at 37°C. For imaging studies of the cell surface of live cells, the Thermonox plastic surface demonstrated superior cell adhesion compared to glass coverslips during scanning by the cantilever tip. For activation experiments, cells were washed with Ringer/BSA buffer (135 mM NaCl, 5 mM KCl, 2 mM $MgCl_2$, 1.8 mM $CaCl_2$, 5 mM glucose and 20 mM HEPES (pH 7.4), and 0.1 mg/ml BSA) and activated with 100 ng/ml antigen (DNP-BSA, Sigma) diluted in Ringer/BSA buffer (Spudich et al., 1992).

For SFM images of the cytoskeleton, unactivated and activated RBL cells were extracted for 2 min with a modified Ringer solution (0.5% Triton-X 100, 2% formaldehyde, 5 mM EGTA, 5 mM $MgCl_2$, 0.5 mM PMSF, 10 μg/ml leupeptin, 50 μg/ml TLCK, and 10 μg/ml pepstatin). After fixation the cells were dehydrated through an ethanol series (30, 50, 70, 85, 95, and 100%, 10 min per dilution) and then treated with hexamethyldisilizane (Electron Microscopy Sciences, Ft. Washington, PA) and air-dried.

Scanning force microscopy

The SFM used for live cell imaging was a Park Scientific Inc. (Sunnyvale, CA) Universal Scanning Probe Microscope (Model SPM-BD2–200) with a 75-μm scanner, modified to have a liquid sample chamber. The sample buffer is trapped between the sample substrate and a glass coverslip, which is held in place above the cantilever by small metal struts. The small volume (~200 μl) of the sample chamber allowed complete and rapid exchange of the sample buffer during activation experiments. Typically, we waited 24 h after plating of the cells before imaging to obtain good cell adhesion on the Thermonox plastic coverslips.

The sample stage was heated during antigen activation to near physiological temperatures (33–37°C), which is necessary to maintain secretion (Metzger et al., 1986). This was accomplished using heater tape wrapped around the microscope base. A small thermocouple affixed near the sample stage monitored the temperature during the experiment. Before activation the base was warmed until thermal equilibrium was reached. The temperature of the inside of the sample chamber loaded with buffer and the temperature of the base were measured to be within 1°C of each other. The surface of the activated cells could be scanned for periods of up to half an hour. Images of the detergent-extracted cytoskeleton and the nuclear surface were obtained using a Park Scientific Autoprobe LS using 100- and 10-μm scanners, respectively.

For live cell imaging, commercial 200-μm-long silicon nitride cantilevers (Park Scientific) with integral pyramidal tips were used, with spring constants of 0.03 N/m. The detergent-extracted cytoskeletons were imaged using 100 μm silicon nitride-coated silicon-tipped cantilevers with a 0.06 N/m spring constant. Placement of the cantilever tip near the cells and observation of the cells during imaging were facilitated by the use of an Olympus model (BH2-UMA) microscope with colinear illumination and a Mitutuyo 50x long working distance objective.

To avoid puncturing the cell membrane during tip approach, the tip was first aimed to make contact with the substrate. Once the tip made contact with the substrate, the scan area was expanded until part of the cell came into view. A screw-driven x-y translation stage allowed movement of the cantilever to a new cell during imaging while the tip was in contact with the sample, thus permitting the imaging of more than one cell per coverslip. The unactivated cells were imaged in Ringer/BSA buffer at 25°C or higher. Cells imaged at near 22°C temperature became less adhesive over the span of an hour. In general, cells displaying one or more processes were more stable and easier to image than flatter, more circular cells that were devoid of processes.

Once contact was made with the substrate, the applied force of the cantilever was reduced to the point where the tip was just in contact with the sample. The forces applied during imaging were kept to a minimum, on the order of 1 nN. When imaging whole cells, high applied forces can result in the cantilever tip damaging the cell membrane and/or detaching the cell from the substratum (Henderson et al., 1992; Parpura et al., 1993). Although the resolution of an SFM image is tightly coupled to the sharpness of the cantilever tip, the use of ultrasharp SFM tips for live cell imaging was avoided, because an ultrasharp tip could exert sufficient pressure on the cell membrane to cause cell lysis.

Live unactivated and activated cells were imaged using SFM with constant height mode (CHM), also refered to as error signal mode (Henderson et al., 1992; Hoh et al., 1993), whereas fixed, detergent-extracted cell preparations were imaged using constant force mode (CFM). Most SFM studies typically use CFM. A CFM image is a three-dimensional map of the sample surface topography produced from the change in z-piezo voltage of the PZT scanner necessary to maintain a constant force applied to the sample as it is Raster-scanned beneath the tip. CHM uses little feedback gain during imaging, so the sample height is held constant by the piezo scanner of the microscope. The output of the split photodiode detector, as opposed to the z-piezo voltage in CFM, is used to produce a map of the change in slope across the sample surface. Previous SFM studies of other types of live cells have demonstrated that CHM can yield images of cytoskeletal ultrastructure with much higher image contrast and definition than CFM (Henderson et al., 1992). Recent work by Hoh et al. (1993) on liver gap junctions also demonstrated that CHM can yield better definition of small protein complexes.

The image contrast of CHM is similar to the first derivative of a topographic CFM image. It is accurate in lateral information, but devoid of height information. For all the live cell image sequences taken with the Park Scientific Universal SPM-BD2–200, the image contrast is defined as follows. A positive slope is defined by black, a negative slope by white, and a flat surface by gray. A ridge or a bump is defined in a CFM image where the image color changes from black to white. For the CHM images of the nuclear surface taken with the Park Scientific Autoprobe LS, the image contrast is essentially defined as the opposite to that described above: a positive slope is denoted by white, a negative slope by black, and a flat surface gray. Because SFM acquires an image by Raster scanning from bottom to top, two points in any image are detected at different points in time. The calculation of the speed of an object requires a correction for the lag in scanning an image. The time difference between each position of an object is derived from the time between each image plus an additional amount to correct for the travel time of the tip to the new object position, in both the vertical and the horizontal directions.

All images were acquired at a pixel density of 256x256 pixels, but at different scan rates. Stored images were baseline-corrected and processed using Park Scientific Autoprobe image processing software. Baseline correction entailed the subtraction of an nth-order polynomial across the whole image on both the x and y axes. Baseline-corrected images were cropped and contrast-adjusted using Adobe Photoshop. Processed images were printed using the direct digital image printing.

DIC microscopy

Cells plated on glass coverslips, grown and activated under conditions described above, were imaged using a Nikon Diaphot inverted microscope modified to have laser confocal differential interference contrast (DIC) optics developed by Dr. Stephen J. Smith of the Cell Sciences Imaging Facility at Stanford University (Francis et al., 1993).

Transmission electron microscopy

For transmission electron microscopy, cells were grown on Formvar-coated nickel grids overnight at 37°C, activated and processed as described above,

except that following extraction, cells were stained with 1% uranyl acetate for 10 min. Extracted cells were imaged with a Philips 200 electron microscope at 80 kV.

RESULTS

SFM and EM of detergent-extracted cells

The cytoskeletal ultrastructure of fixed detergent-extracted preparations of unactivated and activated cells were viewed by EM (Fig. 1, *a* and *b*) and with SFM in CFM mode (Fig. 1, *c* and *d*). The differences between the unactivated and the activated cell images are consistent with the changes in cell morphology seen in DIC images of RBL-2H3 cells (Fig. 2, *a* and *b*), namely the spreading of the cell body. Both SFM and TEM show the activation-induced changes in cytoskeletal organization. In particular, the fine filopodia extending off the cell periphery in the unactivated cell are replaced by a fine filament network in activated cells, and the filament bundles that compose the core of the processes are reorganized (Fig.1). Immunofluorescence microscopy with probes specific to the cytoskeletal filaments F-actin, microtubules, and intermediate filaments have shown that, in both unactivated and activated RBL cells, F-actin is predominately in the cell cortex, whereas the microtubules and the intermediate filaments radiate from the perinuclear region and extend into the processes, making up the bulk of the cytoskeletal filaments within the processes (Spudich et al., 1992).

Amid the fine meshwork of the cytoskeletal filaments observed by TEM are numerous electron dense granules (Fig. 1, *a* and *b*), ~200–500 nm in diameter, which are probably a combination of secretory granules and other vesicles involved in intracellular transport. These granules appear in the DIC images of unactivated and activated RBL cells (Fig. 2, *a* and *b*), concentrated along the center of the processes of the cell in the lower right of the image. In the SFM topographs (Fig. 1, *c* and *d*), these granules appear as bright

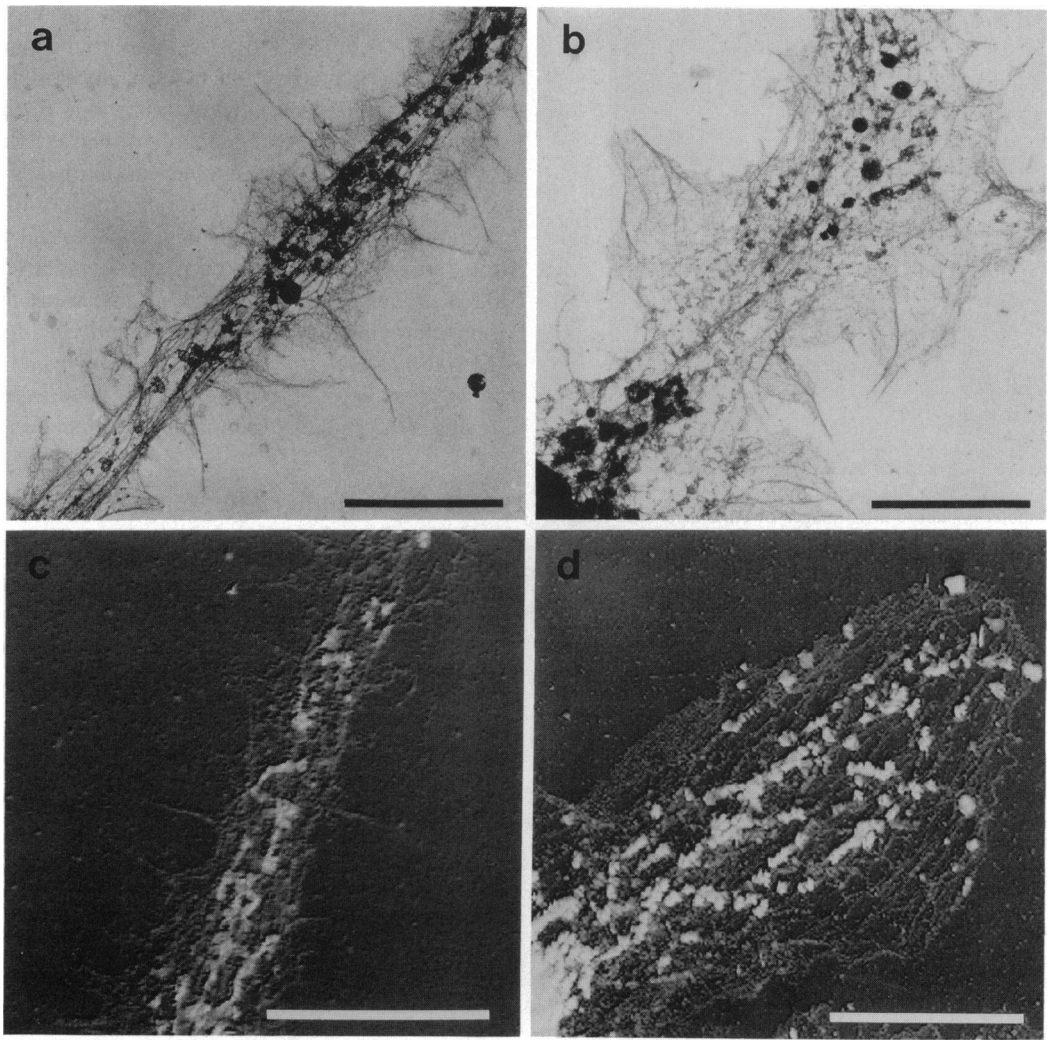

FIGURE 1 Detergent-extracted, unactivated, and activated RBL cells imaged using transmission electron microscopy (*a* and *b*) and SFM in topographic mode in air (*c* and *d*). Reorganization of the cytoskeletal network is evident between *a* and *b*, as it is between *c* and *d*. The round electron-dense structures in *a* and *b* that appear as white spherical structures in *c* and *d*, are granule-like organelles attached to the cytoskeletal network. The topographic images show that the organelles lie primarily on top of the cytoskeletal mesh. Scale bar: (*a*) = 4 μm, (*b*) = 4 μm, (*c*) = 10 μm, and (*d*) = 10 μm.

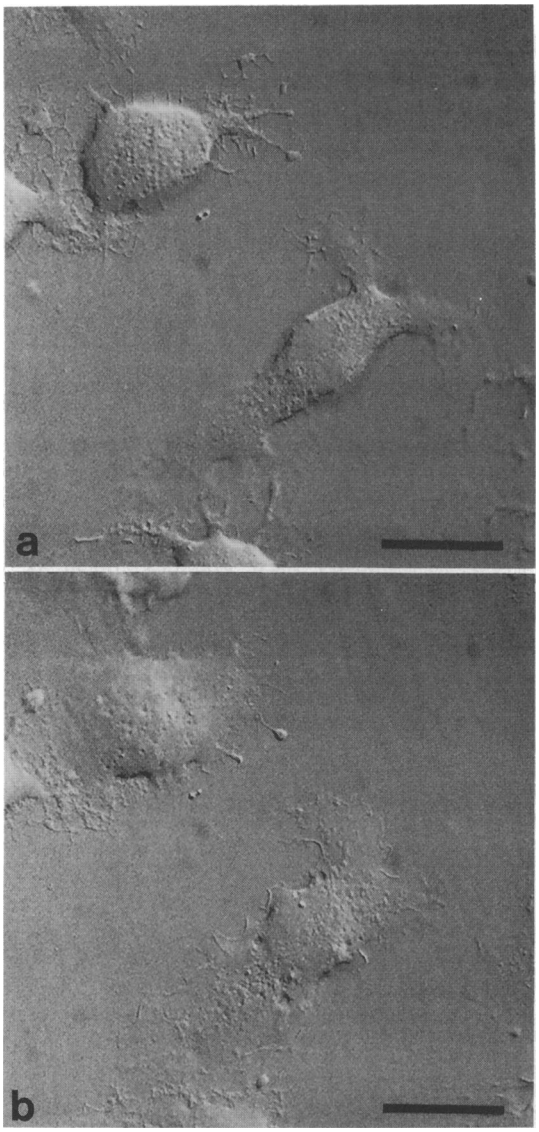

FIGURE 2 Computer-enhanced DIC images of RBL-2H3 cells imaged (*a*) before and (*b*) 10 min after activation with 100 ng/ml DNP-BSA showing the activation-induced flattening, changes of surface structure, and cell morphology. (*a*) Unactivated cells have spherical cell bodies and show multiple processes with fine filopodia. (*b*) Activated cells have undergone considerable flattenening and display many ruffles at the cell periphery. Many granules are apparent near the center of the flattened process of the cell in the lower right. Scale bar = 5 μm.

spherical structures higher than the surrounding cytoskeletal network. The SFM images show that the granules and/or vesicles sit on top of the cytoskeletal network. In contrast, it is difficult with TEM to ascertain whether the granular structures reside within or on top of the cytoskeletal network. The apparent size of the individual filaments in the CFM images is influenced by a combination of factors, such as tip sharpness (Hansma et al., 1993; Venseka et al., 1993), fixation, and extraction conditions. Thus, the single filaments may appear larger in the SFM images than their true size, but the thicker filament arrays are within the range of microtubules and intermediate filament bundles (200–300 nm).

Nuclear pore complexes

We also studied the detergent-extracted nuclear surface with SFM. CFM and CHM images of the nuclei of activated cells (Fig. 3, *a* and *b*, respectively) showed numerous intact nuclear pore complexes (NPCs) scattered across the nuclear surface. The black arrows in Fig. 3 *a* highlight the same corresponding NPCs in Fig. 3 *b*. The relief-like image contrast of the CHM images more clearly defines the outline of the structures than the CFM topographic image. Generally, TEM imaging of the nuclear surface of whole mounted cells is not possible due to the relatively extreme thickness of the nucleus and typically requires spreading of the nuclear membrane across a TEM grid (Akey and Radermacher, 1993; Hinshaw et al., 1992). The images presented here demonstrate the potential for using SFM to explore nuclear surface structure in situ under native conditions.

NPCs were imaged on numerous nuclei and with different tips. A variety of NPC shapes and orientations were observed, so it is unlikely that these structures are caused by any type of tip artifact. The mean diameter of the NPC, 157 ± 6 nm (N = 10), and the approximate mean diameter of the pore, 39 ± 4 nm (N = 10), are close to the values quoted for NPCs seen in other systems (Akey and Radermacher, 1993; Hinshaw et al., 1992). The larger value of the mean outer diameter of the NPC is probably due to the finite sharpness of the tips used. Higher magnification images of the nuclear surface (Fig. 3, *c* and *d*) show the variety of NPC shapes. Although all the NPCs displayed an overall toroidal structure, some NPCs begin to reveal subunit structures (*curved open arrows* in Fig. 3, *c* and *d*), and some appear to have fourfold symmetry (*black arrowheads* in Fig. 3, *c* and *d*). Also in Fig. 3 *d*, one NPC (*open arrowhead*) clearly shows what appears to be an inner plug, a feature reported in *Xenopus* NPC studies (Akey and Radermacher, 1993).

SFM of live quiescent RBL cells

Live unactivated cells (Fig. 4 *a–h*), rich in detail, display surface and subsurface dynamics. Fig. 4 *a–d* are successive images taken at 52-s intervals that show a portion of an unactivated cell surface (at 25°C) near the junction of a process extending from the main cell body. (Note: the image contrast of these images is the opposite of the CHM images shown in the previous section; see Materials and Methods). Many features in the image sequence change from frame to frame. Several spherical structures (*numbered black arrows*) are evident in Fig. 4 *a–d* that are similar in size (~200 nm in diameter) to the small granules visible with DIC microscopy of live unactivated cells (Fig. 2 *a*), and to those seen in detergent-extracted images (Fig. 1 *c*), implying that they are a subsurface structures. They appear to move parallel to linear structures, which can be seen along the axis of the small black arrows in Fig. 4 *a–d*. These linear structures are most probably cytoskeletal filaments. The appearance and disappearance of the granular structures is probably the result of their emergence from and submergence into a deeper part of the cytoplasm.

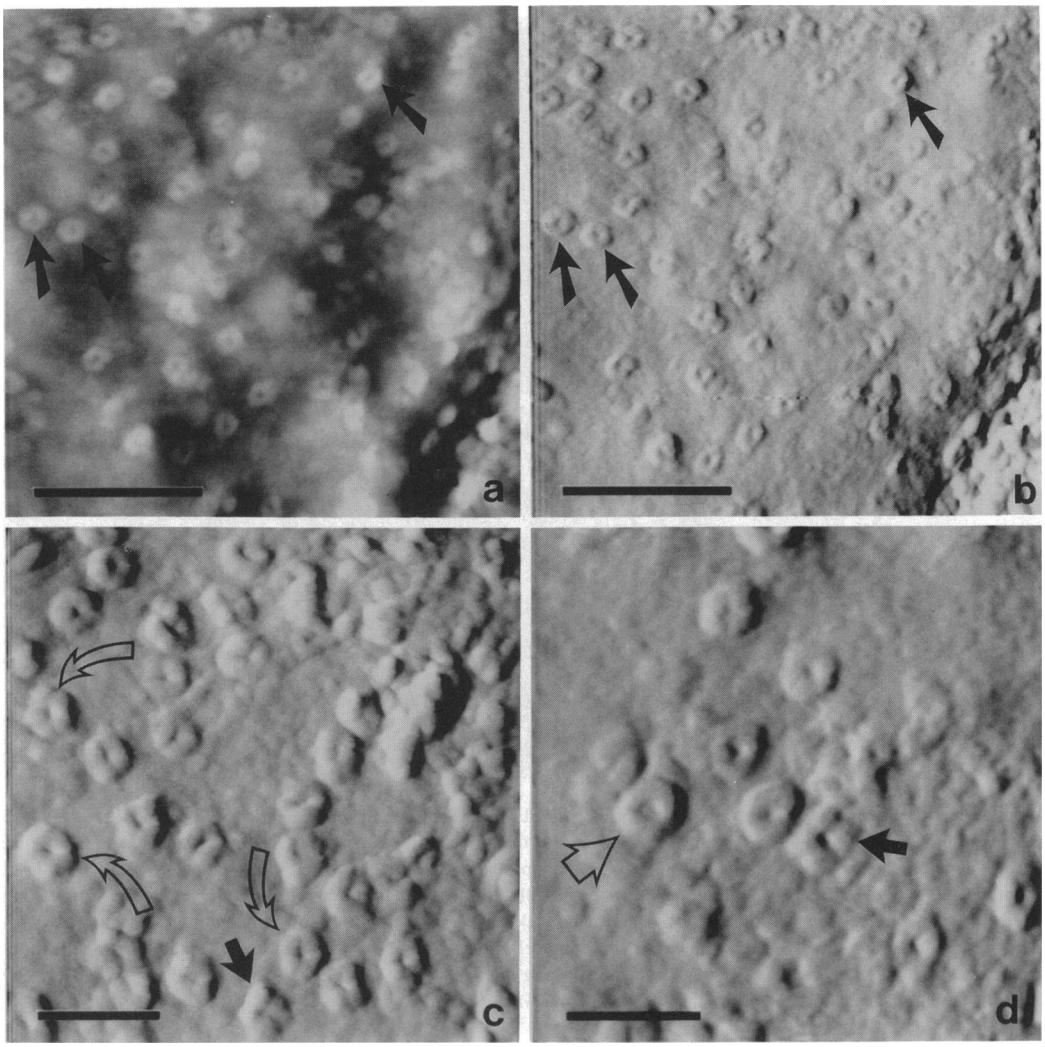

FIGURE 3 SFM images of nuclear pore complexes. (*a*) Low magnification CFM topographic image of the surface of the nucleus of an activated RBL cell showing numerous nuclear pore complexes (NPCs). (*b*) The CHM image of the same area as in *a*. Arrows in *a* and *b* highlight the same NPCs. The CHM image shows the outline of the NPCs more clearly. (*c* and *d*) Higher magnification images of NPCs. Curved open arrows indicate NPCs displaying multiple lobes. Closed black arrowheads indicate NPCs displaying fourfold symmetry. The open arrowhead in *d* highlights an NPC with a central plug. Scale bars: (*a*) = 1.0 μm, (*b*) = 1.0 μm, (*c*) = 0.5 μm, and (*d*) =0.4 μm.

The mean velocity of the granular structures, highlighted in Fig. 4 *a–d* over five frames (*arrow* numbers 1 and 2), are 0.5 ± 0.1 and 0.6 ± 0.3 μm/min respectively. The velocity of these and other organelles in Fig. 4 *a–d* are within the range of velocities reported for intracellular transport (Vale, 1987). This may be due to the proximity of the organelles that we are observing to the plasma membrane. Although the imaging process requires intimate contact of the cantilever tip with the cell surface, the motion of the organelles is independent of the scanning direction of the tip. The organelles have been observed to move opposite to and with the scan direction.

What appears to be a wave (Fig. 4 *a–d*, *open arrowhead pointing to the upper left*) within the cell membrane moves off to the upper left corner of the sequence with a mean velocity of 0.4 ± 0.2 μm/min (N = 5). This velocity is comparable to that of the spherical structures described above and is of the same order of magnitude as the surface velocities seen in other cell systems (Theriot and Mitchison, 1992). These wave-like structures appear to be surface phenomena. Fig. 4 *e–h* demonstrates that SFM can distinguish between waves on the cell surface and underlying cytoskeletal elements.

The image sequence (Fig. 4 *e–h*) shows the central portion of a cell process that runs across the image diagonally from left to right. The linear structures are probably cytoskeletal filaments, because of their spatial orientation and distribution. They resemble the parallel filament arrays visible in Fig. 1, *a* and *c*. Fig. 4, *g* and *h* show what appear to be a collection of surface waves moving over the cytoskeletal filaments. One of the wavefronts (along the axis of the *arrowhead in the upper right of the image*) has moved to the left between Fig. 4, *f* and *g*. By Fig. 4 *h*, the waves have dispersed or have moved out of the scan area. During passage of the waves, the underlying cytoskeletal filaments remain unperturbed, which confirms the location of the waves on the cell surface. Similar

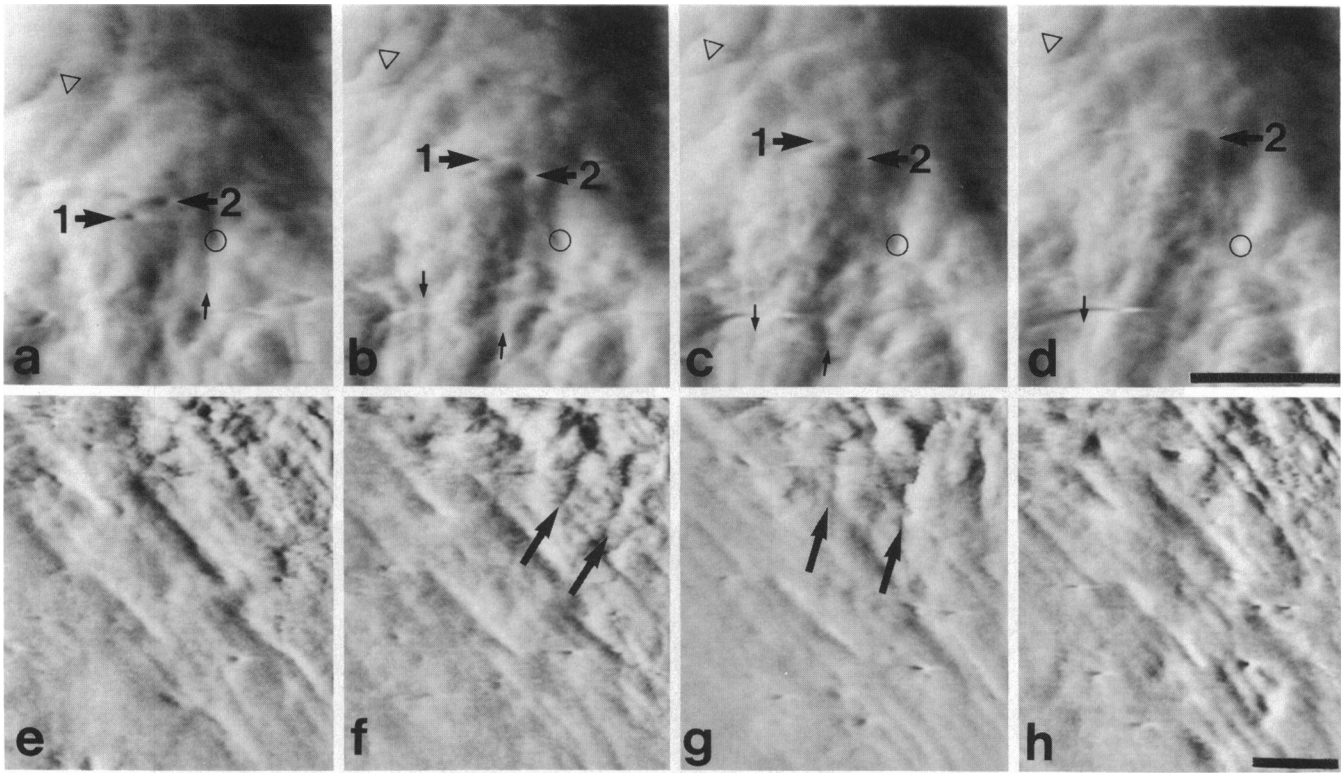

FIGURE 4 Live quiescent RBL cells imaged with SFM at 25°C: (*a–d*) SFM constant height image sequence (5 Hz per scan line or 52 s/image) taken on a cell process near the junction with the nucleus (below the bottom edge of the images) showing surface and subsurface dynamics. Spherical organelle structures ~200 nm in diameter (*numbered black arrows*), which are most probably granules or vesicles, move upward relative to the black circle which remains a stable feature throughout *a–d*. The organelles appear to move parallel to filamentous structures (*small black arrows*) originating from the bottom of the image. What seem to be surface waves within the cell membrane (△) move off to the upper left with each passing frame. (*e–h*) The sequence of CHM images (4 Hz per scan line or 64 s/image) show the center of a long cell process, similar to those in Figs. 2 *c* and 3 *a*. A collection of surface waves passes over underlying cytoskeletal filaments. One of the wavefronts (along the *axes* of the *large black arrows*) moves to the left between *f* and *g*. The underlying cytoskeletal filaments appear unaffected by the passage of the wave (*h*). Scale bars: (*a–d*) = 2 μm, and (*e–h*) = 2 μm.

waves have been observed in other images sequences of quiescent RBL cells.

SFM of live RBL cells responding to receptor activation

We were able to image RBL cells undergoing receptor-mediated activation under physiological conditions. Fig. 5 *a–h* are part of a 26-image sequence recorded over a period of 25 min. The flushing of the sample cell with antigen containing buffer disrupted the imaging process, and thus the images were acquired starting ~2 min after activation. The rapid changes in cell area and structure accompanying activation necessitated imaging over a larger area than that used for the image sequences of the quiescent cells. The stiffening of the cell membrane that occurs upon activation (Liu et al., 1987) appeared to give the activated cells enhanced stability during imaging compared to the quiescent cells, because we could image the activated cells over a longer period.

The sequence in Fig. 5 shows a region of a cell process adjacent to the nucleus, which is located below the lower border of each frame. Early in the sequence, the edges of other cells can be seen diagonally to the right and left of the first. The edges of the central cell in Fig. 5 *a–d* spread over the substrate (*stars to the right and left of the central cell* in Fig. 5 *a*). The right edge of the central cell fills in the small gap between it and the cell on the right (Fig. 5 *b*). The upper left edge of the cell moves across the substrate relative to the three large spherical structures, ~1 μm across (indicated by *open arrowheads pointing to the upper left* in Fig. 5 *b*) at the cell border, two of which appear stationary throughout Fig. 5 *b–d*. Their size and appearance are reminiscent of the large granules seen in the extracted TEM images (see Fig. 1) and near the cell surface in thin section transmission electron micrographs of activated cells (Oliver et al., 1988). When the sequence was viewed in its entirety, many organelles of varying sizes could be seen moving through the cell. One organelle (*arrow pointing to the right*) can be seen moving slowly downward in *a–d*.

During the SFM imaging, the cells were observed with a long working distance optical microscope and clearly displayed the spread appearance of activated cells. Comparing Fig. 5 *a* at 3 min after activation and Fig. 5 *e* at 11 min after activation, there is a noticeable increase in the number of small granules, particularly in the left center of Fig. 5 *e*. The last four images of the sequence Fig. 5 *e–h* show the edges

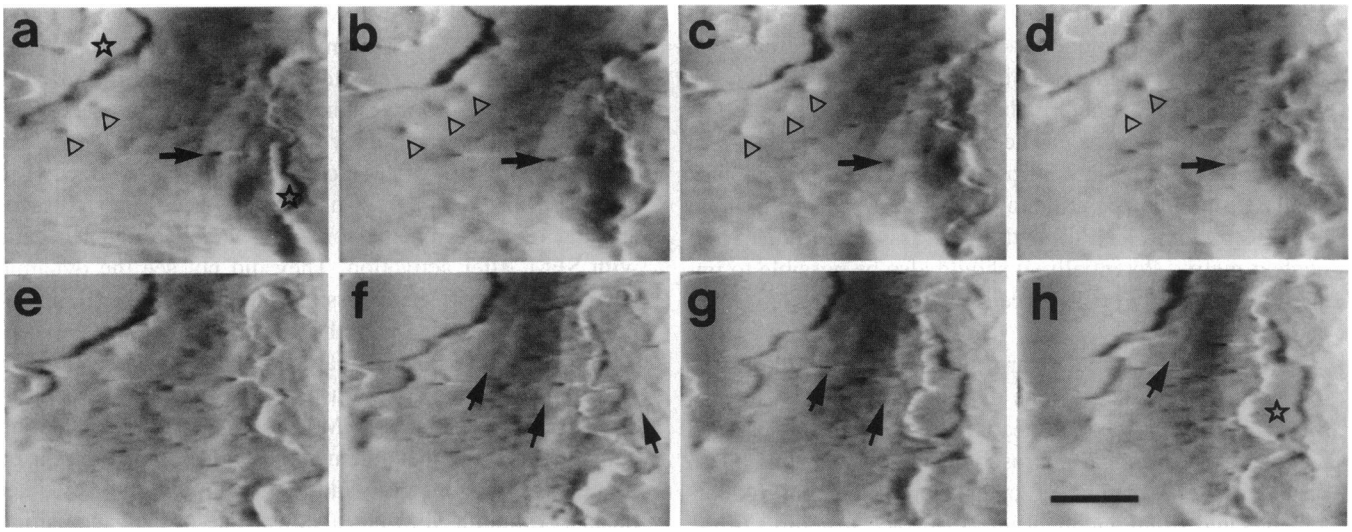

FIGURE 5 Activated RBL cells imaged with the SFM between ~3 min (*a*) and ~11 min (*h*) after antigen-induced activation with 100 ng/ml Ringer BSA at 32–34°C. Succeeding images were taken at intervals of 52 s/image. The image is dominated by a cellular process running diagonally across the image from the lower left to the upper right. The nucleus of this cell lies below the lower left of the image. The edge of a second cell abuts the first to the right and a third to the upper left. (*a–d*) The spreading of the central cell fills in the gap (*star*) between it and the cell to the right. The upper left edge of the central cell moves outward with respect to the three large structures that lie along the cell periphery (*open arrowheads* pointing to the upper left). Numerous small organelles move within the central cell throughout the sequence. One organelle (*black arrow* pointing to the right) moves slowing downward (*a–d*). In the latter half of the sequence (*e–h*), the lamellae of the central cell recedes. Linear structures, which appear to be bundles of cytoskeletal filaments (along the *axis* of the small *black arrowheads* (*f–h*)) move in concert with the cell border as it recedes. All images were taken in CHM, 5 Hz per scan line or 52 s per image. Scale bar = 4 μm.

of the cell receding. This behavior of the cell edge in Fig. 5 *e–h* is probably the result of ruffling or possibly the cell entering the later stages of activation. RBL-2H3 cells undergo very active ruffling at the cell edge during antigen-induced activation. This behavior implies that the changes in cell area observed throughout Fig. 5 are not caused by the action of the tip but result from antigen-induced activation. The linear features visible in the final three images of the sequence in Fig. 5 (along the axis of the black arrows in Fig. 5 *f–h*), which may be microtubule and/or intermediate filament bundles, can be seen drawing closer together concomitant with the receding of the cell border. This is consistent with the behavior of cytoskeletal filaments seen with immunofluorescence in cells toward the end of activation (A. Spudich, unpublished observations).

DISCUSSION

Although other studies have shown that SFM images of large macromolecular structures in air are comparable to images obtained by TEM (DeGrooth and Putman, 1992; Keller et al., 1990; Zenhausen et al., 1992; Allen et al., 1993), we demonstrate here that one can use SFM to image the ultrastructure of the cytoskeleton of detergent-extracted cells with a resolution approaching that of TEM and correlate the structures observed to those seen in SFM images of living cells. Although the TEM and SFM images of the detergent-extracted cells complement each other in the information they provide on cytoskeletal structure, the convenience of imaging extracted cells on a durable substrate such as glass allows rapid characterization of samples. Also, SFM offers the ability to return to the same cell without much concern about sample damage from repeated imaging, as can happen with EM. More importantly, SFM provides information on the relative depth of the organelles within the cytoskeletal matrix. Furthermore, the spherical organelles seen on the extracted cytoskeletal images are similar in size to those observed in the live cell sequences.

Using extracted cell samples, we were able to probe the surface of the nucleus to image NPCs. The samples were prepared without negative staining and metal coatings, so the resulting images are closer to the native structure. The overall dimensions and structure of the NPCs observed were consistent with those reported for image-averaged reconstructions obtained from transmission EM. The differences in the appearances of individual NPCs observed with SFM most probably result from the fact that these are direct images of the surface topography of NPCs in situ, as opposed to differences in electron absorption. The NPCs showed a wide range of shapes, varying from amorphous toroid structures to multilobed rings, some of which clearly showed fourfold symmetry. The smooth ring shape seen in some of the NPCs may be the cytoplasmic ring described in early studies of NPCs from *Xenopus* oocytes (Unwin and Milligan, 1982). The multilobed structures seen on other NPCs in Fig. 3, *c* and *d* could possibly be filaments seen extending from the top of NPCs in recent TEM and SEM studies (Akey and Radermacher, 1993; Hinshaw et al., 1992; Goldberg and Allen,

1992). The different NPC morphologies could be the result of differential extraction, which could explain the observation of the plug in the NPC in Fig. 3 *d*. Alternatively, the variations in NPC structure observed could represent different functional states, as has been suggested by TEM studies (Akey 1990). With sharper tips and selective extraction protocols, it should be possible to obtain additional information on the structure of NPCs and of the associated underlying nuclear matrix. Potentially, it should also be possible to image NPCs directly on RBL cell nuclei in situ under native conditions.

Although movements of organelles and cytoskeletal elements in thin border regions of living cells (Forscher and Smith, 1988; Dabora and Sheetz, 1988) have been observed using enhanced optical microscopies, we have been able to visualize the dynamics of cytoskeletal elements and organelles and simultaneously image surface structures of the relatively thick processes of quiescent cells. We were able to observe the motion of small organelles parallel to what appear to be cytoskeletal filaments, behavior similar to that seen in studies using optical microscopy (Forscher and Smith, 1988; Dabora and Sheetz, 1988). In addition, we can distinguish between waves propagating within the cell membrane from movements of organelles and cytoskeletal elements below the cell surface. Furthermore, from the image sequences we can derive the velocities of the structures observed and correlate them to data from optical microscopy studies.

The ability to detect surface waves within the cell membrane reinforces the notion that the mechanism of visualization of sub-surface cytoskeletal structures with SFM results from the cantilever tip pressing on, but not breaching, the cell membrane (Henderson et al., 1992). The surface waves observed in the quiescent cells were very resilient to the scanning action of the tip. Large cytoplasmic wave-like structures have been observed previously with optical microscopy (Sorrano and Bell, 1982; Couchman and Lenn, 1985). Kasas et al. (1993) also observed individual wave-like structures within the cell membrane of lung cells with SFM, which were much larger in scale than those observed in Fig. 4. The events we observed in the quiescent RBL cells consisted of multiple wavefronts traversing within the cell membrane independent of underlying cytoskeletal filament arrays. The velocities of the wave-like structures and organelles in Fig. 5 (*a–d*) are of the same order of magnitude as the velocities measured for photo-labeled actin networks in fibroblasts (Theriot and Mitchison, 1992).

The spreading of the cell edges in response to crosslinking of the IgE-receptor at the cell surface imaged by the SFM was consistent with the DIC images of activated RBL cells. The increased granulation observed between Fig. 5, *a* and *e* probably resulted from the flattening of the cell, which results in more granules being pushed closer to the cell surface thus making them accessible to the cantilever tip. The DIC images of the activated cells display similar behavior such as the cell in the lower right of Fig. 2 *b*. The imaging of the activated cells in Fig. 5 shows that SFM can acquire and resolve surface details simultaneously without the need for integration of successive images. The lamellae at the spreading cell edge were resilient to the repeated action of the tip and were clearly resolved. The resistance of the edges of the activated cells to repeated scanning by the SFM tip may be due to the increased stiffness of the activated RBL cell surface (Liu et al., 1987). Previously, Chang et al. (1993) imaged cytoskeletal filaments on the spreading lamellae of RBL cells with SFM, after activation. They did not see the dynamic changes we report here, possibly due to the lower temperature and smaller scan area they used for imaging.

We have used SFM to image live cells, at relatively high resolution and image contrast, undergoing changes due to specific external signals. SFM not only provides information complementary to that obtained by standard techniques used for cell imaging, but also yields data not measurable by other means. Although SFM has a slower rate of data acquisition than video microscopy, it can image and distinguish between events at the surface and just below the cell surface. Furthermore, with SFM we have probed the ultrastructure of fixed cell preparations without the need for staining or metal coating, while yielding results comparable and complementary to transmission electron microscopy. Such flexibility of use is not possible with any other single instrument. Because of these diverse capabilities, SFM has the potential to become a very powerful tool for the study of cell structure and dynamics.

We would like to thank Profs. James A. Spudich and Calvin F. Quate for their support on this research and comments on this manuscript. We want to extend special thanks to Dr. Sung Park for the use of the Park Scientific Autoprobe LS. We wish to thank Dr. Joan T. Wrenn for help with the transmission electron microscopy. We also thank Marco Tortonese for the gift of the silicon nitride-coated Si tips. Finally, we would like to thank Dr. Suzanne Pfeffer for the use of the cell culture facility.

This work was supported by National Institutes of Health grant M 30387 (to J. A. Spudich) and National Science Foundation ECS 89175552 (to C. F. Quate). D. Braunstein is supported by National Institutes of Health postdoctoral fellowship (AR088202–03). A. Spudich is supported by a grant from the Program in Molecular and Genetic Medicine at the Beckman Center, Stanford University.

REFERENCES

Akey, C. W. 1990. Visualization of transport-related configurations of the nuclear pore transporter. *Biophys. J.* 58:341–356.

Akey, C. W., and M. Radermacher. 1993. Architecture of Xenopus nuclear pore complex revealed by cryo-electron microscopy. *J. Cell Biol.* 122: 1–19.

Allen, M. J., X. F. Dong, T. E. O'Neill, P. Yau, S. C. Kowalczykowski, J. Gatewood, R. Balhorn, and E. M. Bradbury. 1993. Atomic force microscope measurements of nucleosome cores assembled along defined DNA sequences. *Biochemistry.* 32:8390–8396.

Binnig, G., C. F. Quate, and C. Gerber. 1986. The atomic force microscope. *Phys. Rev. Lett.* 56:930–933.

Braunstein, D., J. A. Spudich, and C. F. Quate. 1993. Atomic force microscopy of covalently and electrostatically immobilized F-actin. *Biophys. J.* 64:246a. (Abstr.)

Chang, L., T. Kious, M. Yorgancioglu, D. Keller, and J. Pfeiffer. 1993. Cytoskeleton of living, unstained cells imaged by scanning force microscopy. *Biophys. J.* 64:1282–1286.

Couchman, J. R., and M. Lenn. 1985. Coupling of cytoskeletal functions for fibrolast locomotion. *Eur. J. Cell Biol.* 36:182–194.

Dabora, S. L., and M. P. Sheetz. 1988. Cultured cell extracts support organelle movements on microtubules in vitro. *Cell Motil. Cytoskel.* 10: 482–495.

Degrooth, B. G., and C. A. J. Putman. 1992. High-resolution imaging of chromosome-related structures by atomic force microscopy. *J. Microscopy-Oxford.* 168:239–247.

Forscher, P., and S. J. Smith. 1988. Actions of cytochalasins on the organization of actin filaments and microtubules in a neuronal growth cone. *J. Cell Biol.* 107:1505–1516.

Francis, C. L., T. A. Ryan, B. D. Jones, S. J. Smith, and S. Falkow, S. 1993. Ruffles induced by *Salmonnella* and other stimuli direct macropinocytosis of bacteria. *Nature.* 364:639–642.

Goldberg, M. W., and T. D. Allen. 1992. High resolution scanning electron microscopy of the nuclear envelope-demonstration of a new, regular, fibrous lattice attached to the baskets of the nucleoplasmic face of the nuclear pores. *J. Cell Biol.* 119:1429–1440.

Hansma, H. G., M. Bezanilla, F. Zenhausern, and M. Adrian. 1993. Atomic force microscopy of DNA in aqueous solutions. *Nucleic Acids Res.* 21: 505–512.

Henderson, E., P. G. Haydon, and D. S. Sakaguchi. 1992. Actin filament dynamics in living glial cells imaged by atomic force microscopy. *Science.* 257:1944–1946.

Hinshaw, J. E., B. O. Carragher, and R. A. Milligan. 1992. Architecture and design of the nuclear pore complex. *Cell.* 69:1133–1141.

Hoh, J., G. E. Sosinsky, J. P. Revel, and P. K. Hansma. 1993. Structure of the extracellular surface of the gap junction by atomic force microscopy. *Biophys. J.* 65:149–163.

Hörber, K. H., W. Haberle, F. Ohnesorge, G. Binning, H. G. Liebich, H. G. Czerny, H. Mahnel, and A. Mayr. 1992. Investigation of living cells in the nanometer regime with the scanning force microscope. *Scanning Microscopy.* 6:919–930.

Kasas, S., V. Gotzos, and M. R. Celio. 1993. Observation of living cells using atomic force microscopy. *Biophys. J.* 64:539–544.

Keller, R. W., D. J. Keller, D. Bear, J. Vasenka, and C. Bustamante. 1992. Electrodeposition procedure of E. coli RNA polymerase onto gold and deposition of E. coli RNA polymerase onto mica for observation with scanning force microscopy. *Ultramicroscopy.* 42–44:1173–1180.

Liu, Z.-Y., J. I. Young, and E. L. Elson. 1987. Rat basophilic leukemia cells stiffen when they secrete. *J. Cell Biol.* 105:2933–2943.

Lyubchenko, Y. L., P. Oden, D. Lampner, S. M. Lindsay, and K. A. Dunker. 1993. Atomic force microscopy of DNA and bacteriophage in air, water and propanol: the role of adhesion forces. *Nucleic Acids Res.* 21: 1117–1123.

Metzger, H., G. Alcaraz, R. Holman, J.-P. Kinet, V. Pribula, and R. Quarto. 1986. The receptor with high affinity for immunoglobulin E. *Annu. Rev. Immunol.* 4:419–470.

Murray, M. N., H. G. Hansma, M. Bezanilla, T. Sano, D. F. Ogletree, W. Kolbe, C. L. Smith, C. R. Cantor, S. Spengler, and P. K. Hansma. 1993. Atomic force microscopy of biochemically tagged DNA. *Proc. Natl. Acad. Sci. USA.* 90:3811–3814.

Oliver, J. M., J. C. Seagrave, R. F. Stump, J. R. Pfeiffer, and G. G. Deanin. 1988. Signal transduction and cellular response in RBL-2H3 mast cells. *Prog. Allergy.* 42:185–245.

Parpura, V., P. G. Haydon, and E. Henderson. 1993. Three-dimensional imaging of living neurons and glia with the atomic force microscope. *J. Cell Sci.* 104:427–432.

Rees, W. A., R. W. Keller, J. P. Vesenka, G. Yang, and C. Bustamante. 1993. Evidence of DNA bending in transcription complexes imaged by scanning force microscopy. *Science.* 260:1646–1649.

Siraganian, R. P., A. McGivney, E. L. Barsumian, F. T. Crews, F. Hirata, and J. Axelrod. 1982. Variants of the rat basophilic leukemia cell line for the study of histamine release. *Fed. Proc.* 41:30–34.

Soranno, T., and E. Bell. 1982. Cytostructural dynamics of spreading and translocating cells. *J. Cell Biol.* 95:127–136.

Spudich, A., T. Meyer, and L. Stryer. 1992. Association of the beta isoform of protein kinase C with vimentin filaments. *Cell Motil. Cytoskel.* 22: 250–256.

Stossel, T. 1993. On the crawling of animal cells. *Science.* 260:1086–1094.

Theriot, J. A., and T. J. Mitchison. 1992. Comparison of actin and cell surface dynamics in motile fibroblasts. *J. Cell Biol.* 119:367–377.

Unwin, P. N. T., and R. A. Milligan. 1982. A large particle associated with the perimeter of the nuclear pore complex. *J. Cell Biol.* 93:63–75.

Vale, R. D. 1987. Intracellular transport using microtubule-based motors. *Annu. Rev. Cell Biol.* 3:347–378.

Venseka, J., S. Manne, R. Giberson, T. Marsh, and E. Henderson. 1993. Colloidal gold particles as an incompressible atomic force microscope imaging standard for assessing the compressibility of biomolecules. *Biophys. J.* 65:992–997.

Weisenhorn, A. L., B. Drake, C. B. Prater, S. A. Gould, P. K. Hansma, F. Ohnesorge, M. Egger, S. P. Heyn, and H. E. Gaub. 1990. Immobilized proteins in buffer imaged at molecular resolution by atomic force microscopy. *Biophy. J.* 58:1251–1258.

Zenhausern, F., M. Adrian., B. ten Heggeler-Bordier, R. Emch, M. Jobin, M. Taborelli, and P. Descouts. 1992. Imaging of DNA by scanning force microscopy. *J. Struct. Biol.* 108:69–73.